Scientific Report

Regarding the Project Implementation during January - December 2015

Phase V: Laser pyrolysis process optimization for the synthesis of magnetic powders based on TiO_2 embedded in carbosiloxane polymers and the comparation of the results with the data from literature regarding the magnetic properties:

1. Experimental optimization

2. Comparative study on the synthesyis method efficiency for catalytic properties demonstration

The optimization of the laser oxidative pyrolysis synthesis process in this Phase was focused on enhancement of the resulted nanopowders properties aiming both photocatalytic and magnetic properties. For tis goal, the following parameters were varied:

- the injection geometry of the precursors in the reaction zone
- the flows of precursors – resulting samples with various $TiO_2/FeO_x/SiO_2$ ratios
- the laser power density during the synthesis process

Vartiation of the injection geometry of precursors in the pyrolysis flame

Two different geometries were tested for the silicon precursor introduction in the reaction zone: either through the central nozzle (Fig. 1a) either through external annular one (Fig 1b). The iron precursor wqas introduced though the inner nozzlefor both configurations, whereas on the

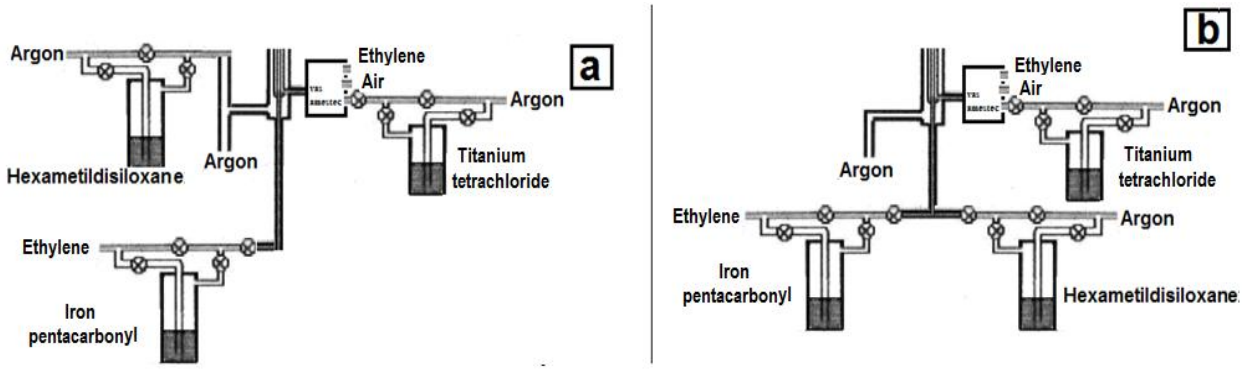

Fig.1. The schematic represenation of the two precursors injection geometries

intermediary annuar nozzle, the precirsor required for thew obtaining of TiO_2 ($TiCl_4$ and O_2 as synthetic air) . The ethylene sensitizer was introduced in bith geometries through the inner tubular and intermediate annular nozzle.

For each geometry, the $Fe(CO)_5$ (iron precursor) flow was varied to observe their influence on the magnetic (and eventually to photocatalytic) properties of titania-based resulted nanopowders.

Table.1. Synthesis parameters and the elemental composition (from EDX measurements) with iron precursor flow variation – geometry a

Proba	$\Phi_{Aircond.}$ [sccm]	$\Phi_{Ar/ H2O/O2}$ [sccm]	$\Phi_{Ar/ TiCl_4}$ [sccm]	Φ_{Ar} [sccm]	Φ_{C2H4} [sccm]	$\Phi_{C2H4/ Fe(CO)5}$ [sccm]	P [W]	EDAX(at%)					
	Duza externa		Duza intermediara			Duza interna		Fe	Ti	O	Si	C	Total
ITP-18	1500	100	150	450	30	10	350	2	13.6	59.4	9.6	15.4	100
ITP-11	1500	100	150	450	30	5	350	1.8	13.3	56.6	9.4	18.9	100
ITP-12	1500	100	150	450	30	5 fara Fe	310	-	15.8	60.6	8.7	14.9	100

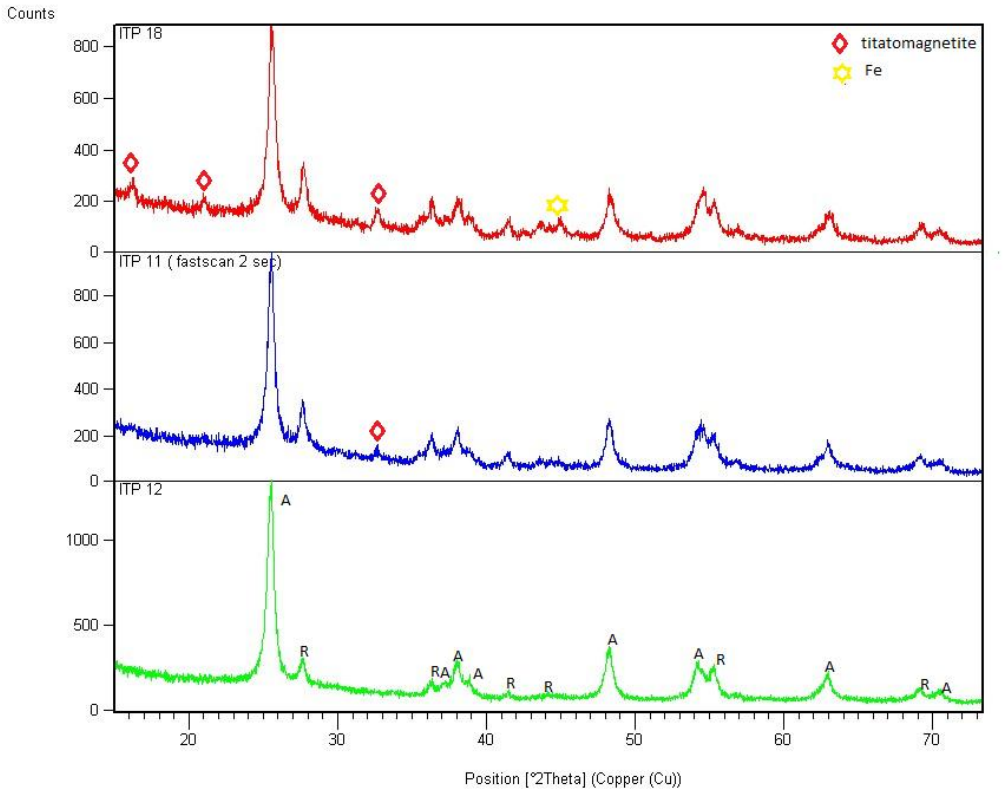

Fig. 2. Superposed X-ray diffractograms for ITP 18, ITP 11, ITP 12 samples

Tabelul 2. XRD results coresponding to Fig. 2.

Sample	TiO2			
	A (%)	R(%)	D_A (nm)	D_R(nm)
ITP 18	81.79	18.21	13	9
ITP 11	80.96	19.04	15	8
ITP 12	89.19	10.81	16	6

Table 3. Synthesis parameters and the elemental composition (from EDX measurements) with iron precursor flow variation – geometry b

Proba	$\Phi_{Ar conf}$ [sccm]	$\Phi_{Ar TiCl4}$ [sccm]	Φ_{Ar} [sccm]	Φ_{C2H4} [sccm]	$\Phi_{C12H47Fe(CO)3}$ [sccm]	$\Phi_{Ar HMDSO}$ [sccm]	P [W]	EDAX(at%)					
								Fe	Ti	O	Si	C	Total
	Duza externa	Duza intermediara			Duza interna								
ITP-13	1500	150	450	30	10	20	310	3	12	60.5	13.2	11.3	100
ITP-14	1500	150	450	30	5	20	310	1.4	14.6	65.7	11.1	7.2	100
ITP-15	1500	150	450	30	5 fara Fe	20	310	-	10.1	67.1	14.3	8.5	100

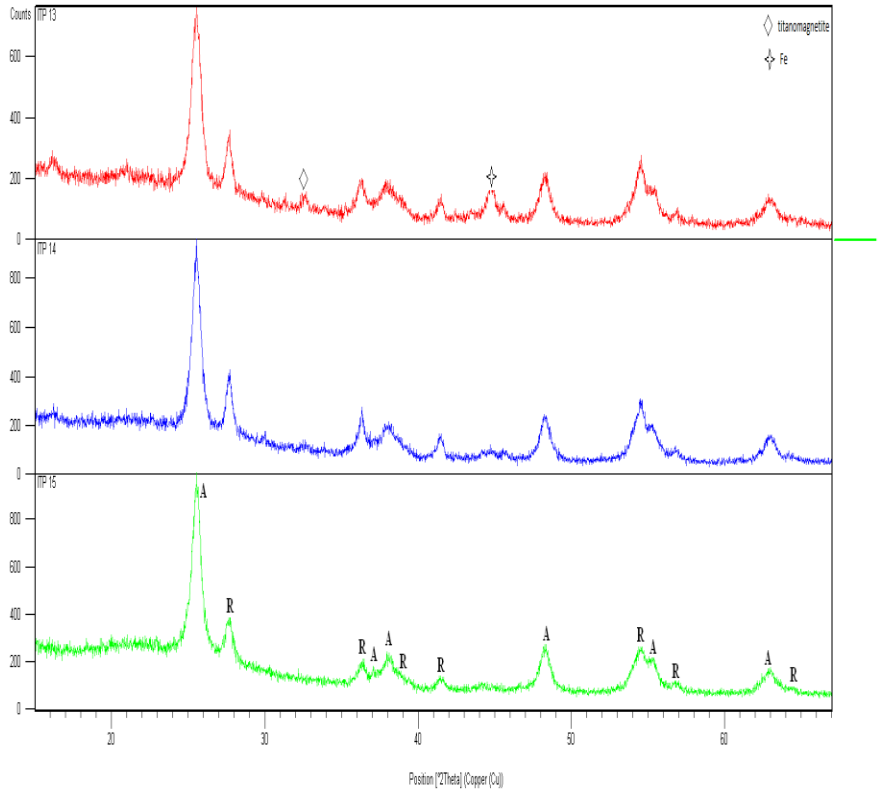

Fig. 3. Superposed X-ray diffractograms for ITP 13, ITP 14, ITP 15 samples

Table 4. XRD results coresponding to Fig. 3.

Sample	TiO_2			
	A (%)	R(%)	D_A (nm)	D_R(nm)
ITP 13	71	29	11	18
ITP 14	70.1	29.9	13	28
ITP 15	76.55	23.45	12	14

The variation of the ratio between TiO_2 and Fe precursors– resulting samples with different TiO_2/Fe/ SiO_2 content

Table 5. Variation of ratios between TiO_2 and Fe precursors - geometry a

Proba	$\Phi_{Ar\ conf}$ [sccm]	$\Phi_{Ar\ HMDSO}$ [sccm]	$\Phi_{Ar\ TiCl4}$ [sccm]	Φ_{Air} [sccm]	Φ_{C2H6} [sccm]	$\Phi_{C5H5Fe(CO)3}$ [sccm]	P [W]	EDAX(at%)					
	Duza externa		Duza intermediara			Duza interna		Fe	Ti	O	Si	C	Total
ITP-8	1500	100	70	200	30	20	350	8	10.3	49.8	6.7	25.2	100
ITP-10	1500	100	100	300	30	20	350	8.6	14.7	54.2	5	17.5	100
ITP-9	1500	100	100	300	30	10	350	3.3	12.3	57.3	8.2	18.9	100
ITP-11	1500	100	150	450	30	5	350	1.8	13.3	56.6	9.4	18.9	100
ITP-12	1500	100	150	450	30	5 fara Fe	310	-	15.8	60.6	8.7	14.9	100

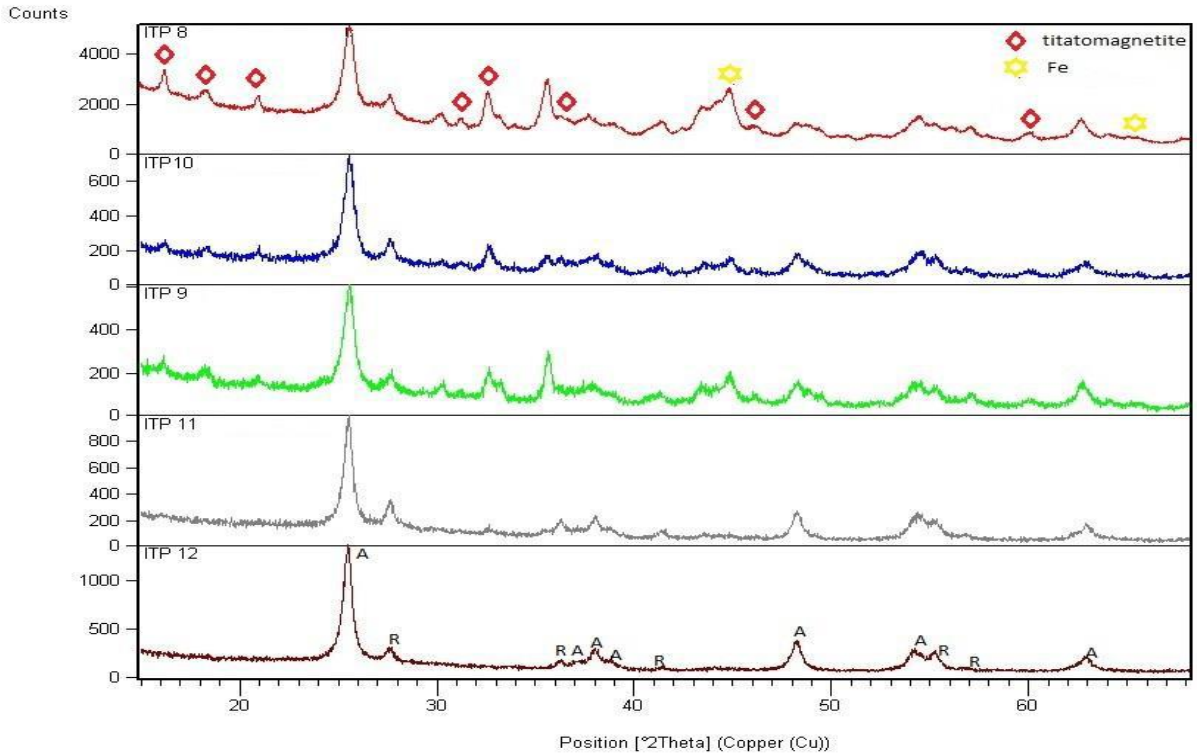

Fig. 4. Superposed X-ray diffractograms for ITP 8...12 samples

Table 6. XRD results coresponding to Fig. 4.

Sample	TiO_2			
	A (%)	R(%)	D_A (nm)	D_R(nm)
ITP 8	78.58	21.42	12	8
ITP 9	82.18	17.82	14	9
ITP 10	81.79	18.21	13	9
ITP 11	80.96	19.04	15	8
ITP 12	89.19	10.81	16	6

Laser power density variation during synthesis

Tabelul 7. *Laser power variation (Fe(CO_5 min. flow, $TiCl_4$ max. flow)-geometry b*

Proba	$\Phi_{Ar\,sint}$ [sccm]	$\Phi_{Ar\,TiCl_4}$ [sccm]	Φ_{Air} [sccm]		$\Phi_{C_2H_4}$ [sccm]	$\Phi_{Ar\,Fe(CO)_5}$ [sccm]		P [W]	EDAX (at%)					
									Fe	Ti	O	Si	C	Total
	Duza externa	Duza intermediara				Duza interna								
ITP-16	1500	150	450	30		5	20	250	1.1	13.1	67.2	8.6	10	100
ITP-17	1500	150	450	30		5	20	280	1.7	10.1	65.8	16.1	6.3	100
ITP-14	1500	150	450	30		5	20	310	1.4	14.6	65.7	11.1	7.2	100
ITP-15	1500	150	450	30		5 fara Fe	20	310	-	10.1	67.1	14.3	8.5	100

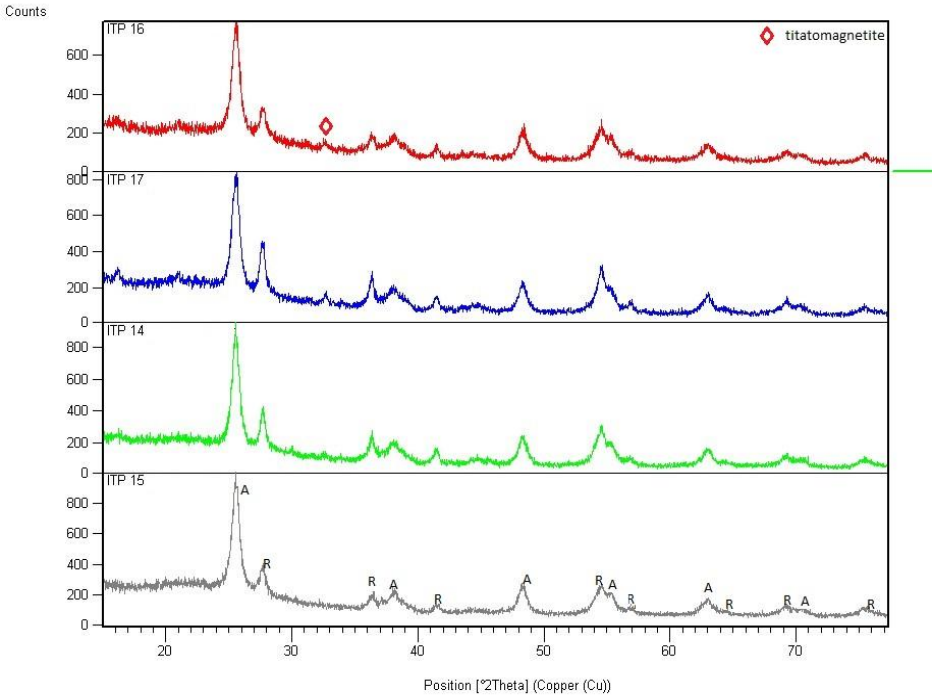

Fig. 5. Superposed X-ray diffractograms for ITP 14, ITP 15, ITP 16, ITP 17 samples

Table 8. XRD results coresponding to Fig. 5.

Sample	TiO_2			
	A (%)	R(%)	D_A (nm)	D_R(nm)
ITP 16	76.55	24.41	12	14
ITP 17	63.07	36.93	14	22
ITP 14	70.1	29.9	13	28
ITP 15	76.55	23.45	12	14

XRD analyses show the presence of a mixture of the main titania phases – rutile and anatase, where thw anatase phase is the mean one which is beneficial for photocatalytic applications. The samples with high atomic Si% show also a very weak and large peak at XRD, centred ~2θ= 23°, corresponding to amorphous SiO_2. No XRD peaks of crystalline graphite can be observed in any of the samples, indicating their amorphous form. Also, the enhancement of the iron precursor flow introduced in the reaction zone induces a reduction of the anatase percent and an increasing of those of rutile, accompanied with the appreearance of supplementary phases tentatively ascribed to titanomagnetie/titanomaghemite. Generally, the sample obtained using the **b** geometry have a higher atomic Si content towards those obtained in **a** geometry due to the dilution of silicon precursor with high amount of confinment Ar through extrenal annular nozzle in the configuration **a**. Also, the geometry **a** resulted samples have a clear higher carbon content compared with those resuletd from geometry **b**. By keeping the titania precursors flow constant, by increasing those of iron precursor, an increasing of atomic iron content can be observed in the resulted nanopowders. In the samples with the highest atomic % of Fe, the metallic αFe phase was identified, which can be beneficial for the magnetic properties of those powders.

SEM analyses

The scanning electronn microscopy SEM images from some of the nanopawders obtained in the two different injection geometries can be seen in Fig.6. Aggregates of nanometric size particles , which are in agreement with the crystallite seize from XRD can be seen.

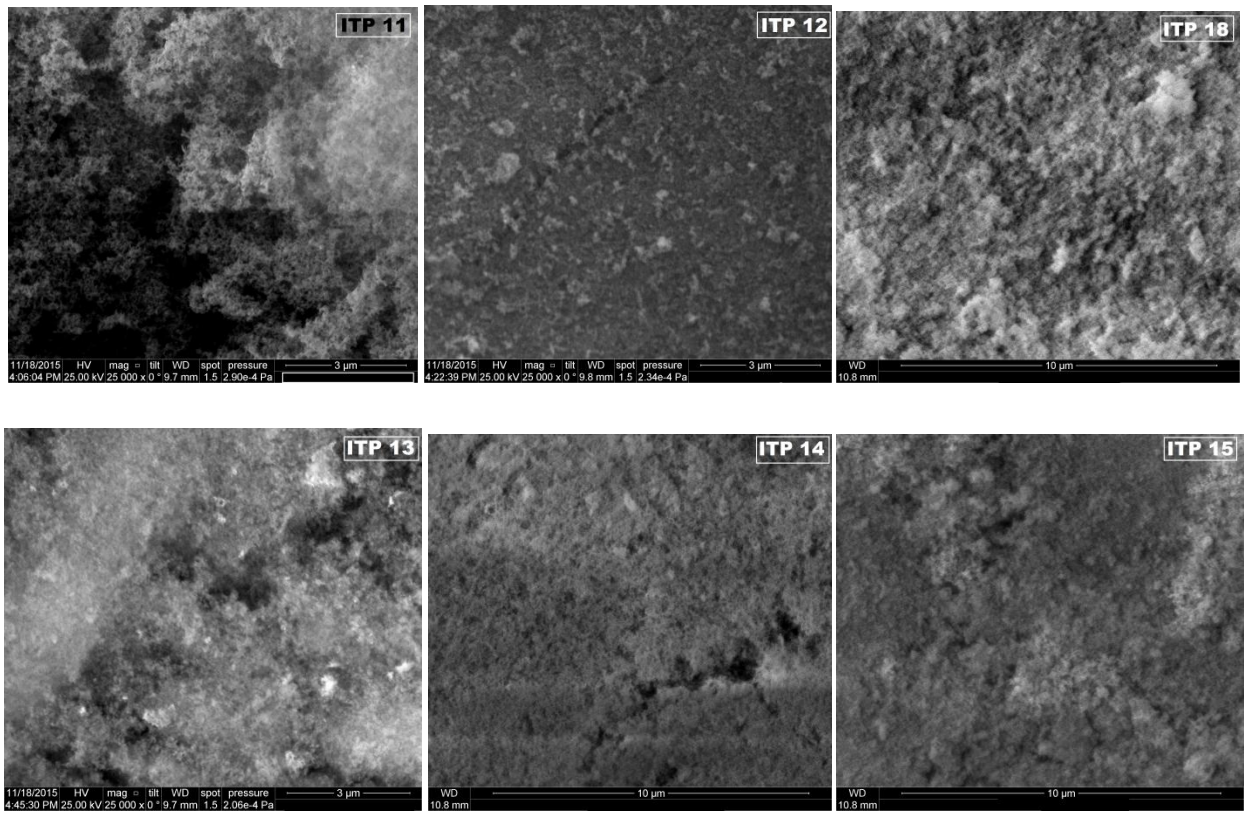

Fig.6. SEM images fron the ITP-11, ITP 12, ITP18 (geometry a) si ITP-13, ITP 14, ITP15 (geometry b) nanopowders

UV-Vis spectroscopy-derived characterization

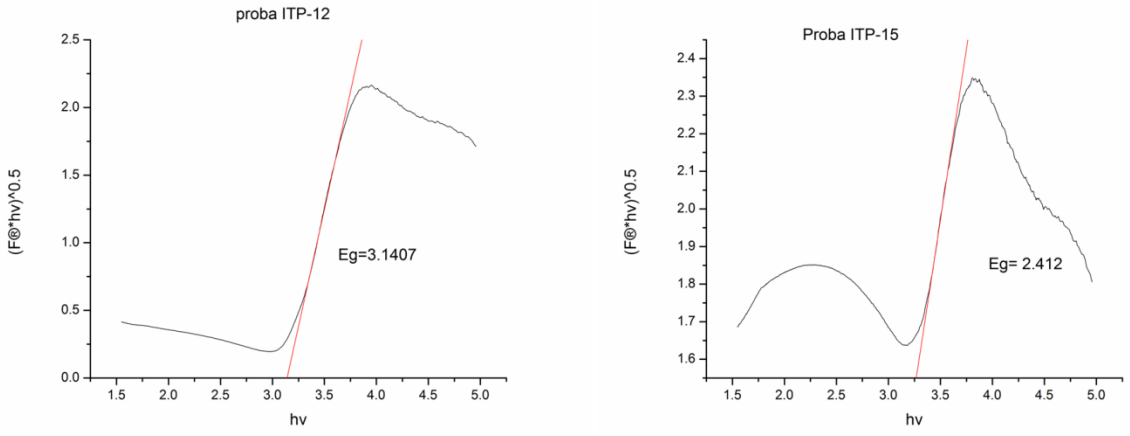

Fig.7. Indirect transition absorbance spectra $F(R)^{1/2}$ vs E (eV) for reference ITP 12 si ITP 15samples

Indirect transition absorbance spectra for ITP12 TiO_2/SiO_2 type sample obtained using the geometry **a** (**Fig.7.)** has a similar shape with those of a commercial pure TiO_2 sample Degussa P25, having in the same time a close value of the bangap energy: 3.2 eV. Concerning the ITP 15 sample obtaineds using geometry b (also obtained without Fe precursor and having a higher silicon atomic content than ITP12), the shape of the spectrum (as presented in Fig. 7 right part) is different, presenting in the same time a much lower bandgap compared with those of ITP 12 si P25, indicating an enhancement of absorbtion in the vizible domain.

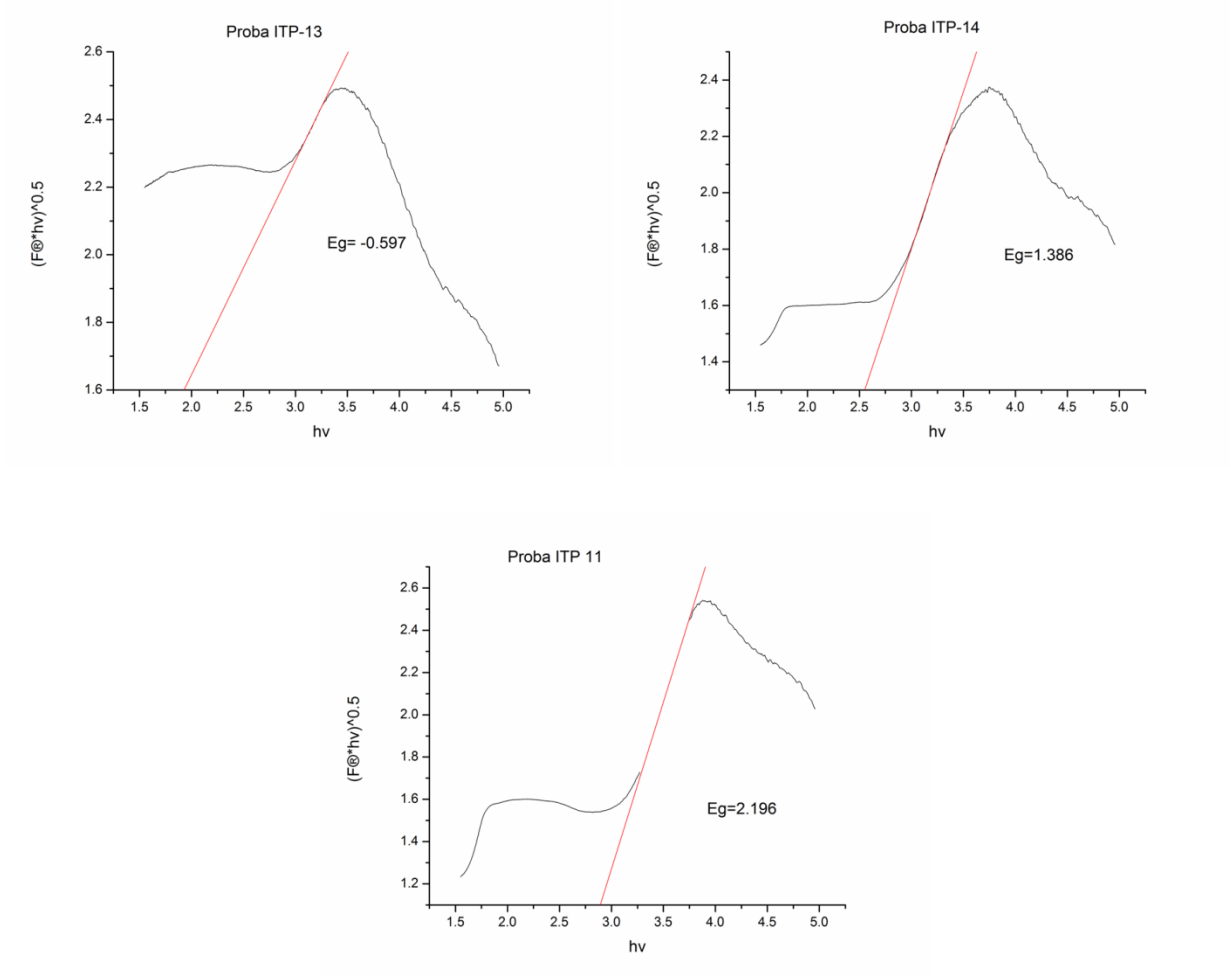

Fig.8. Indirect transition absorbance spectra $F(R)^{1/2}$ vs E (eV) for: ITP 11, ITP 13 si ITP 14 Fe-containing samples

The samples obtained using a low iron precursor flow (5 sccm of $Fe(CO)_5$) – ITP11 (geometry **a**) and ITP 14 (geometry **b**) have both a lower bandgap (Fig.8) when comparing with those of the

Degussa P25 reference (3.2 eV).This fact can allow the coclusion that the Fe introduction seems to be benefical to a bettere absorbtion towards visible light of the TiO_2/SiO_2-baseed nanopaowders. However, the introduction of a higher iron precursor flow (10 sccm de $Fe(CO)_5$) – sample ITP13 (geometry **b**) is translated into a material with apparent negative bandgap which can't be found in the specific literature dedicated to photocatalytic semiconductors (negative bandgap arising from overlapping conduction and valence bands). This behaviour can be related with the presence of metallic iron (which was found in the X-ray diffractogram of this sample), iron which can also induce magneto-responsive properties to this powder.

Magnetic characterizations

Selected samples were magnetically characterized (hysteresis curves, FC-ZFC and Mossbauer. For Mossbauer spectroscopy the ITP_11 (Fig. 9.) si ITP10 (Fig. 10) spectra are shown

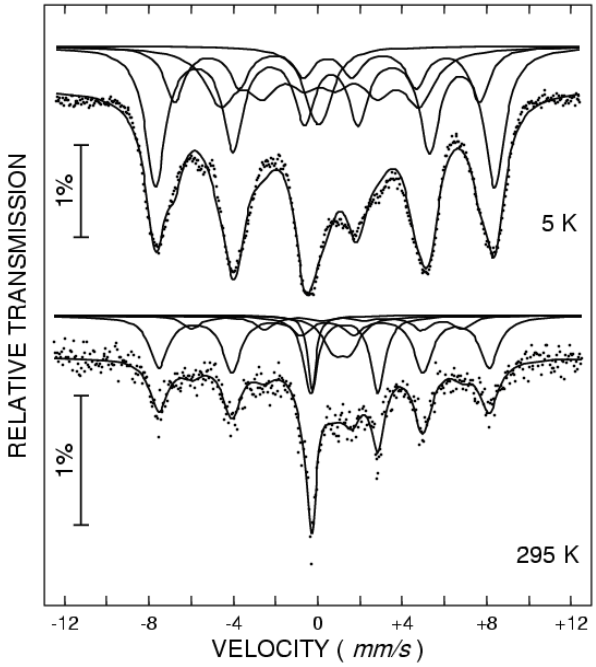

Fig.9. Mossbauer spectra for ITP-11 sample

The Mossbauer measurements highlight the existence of magnetically ordered species from their sextets, more visible at very low temperature (5 K) whre their areas are majority.

The sextets with absorption lines at velocities ~ +/- 8 mm/s can be attributed to iron oxides with spinelic structure, where the iron can be found as Fe^{3+} with high spin (S= 5/2). The amount of those spinelic phases can be extracted from their peaks relative areas 66% at 5 K and, 57% at 295 K, respectively for ITP-1 sample and 69 % at 5 K for ITP-10 sample.

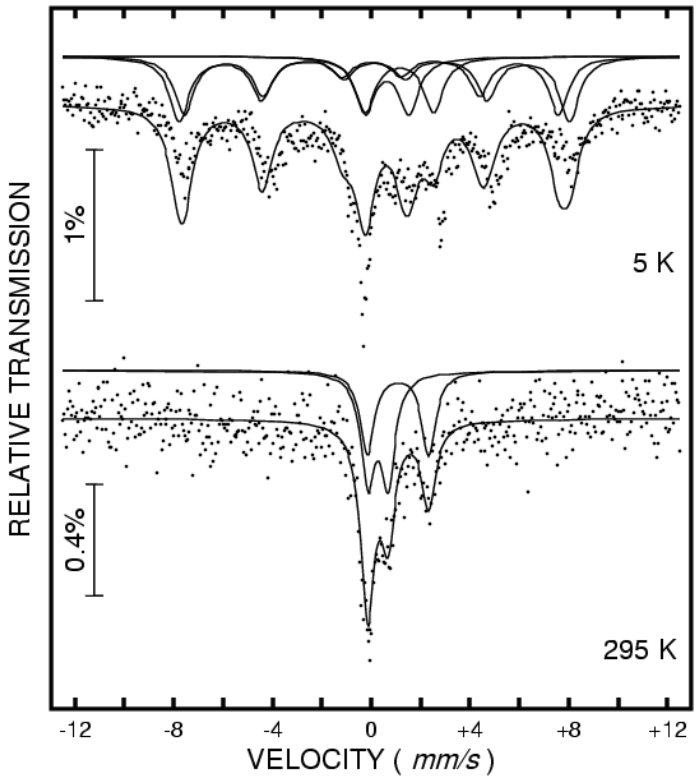

Fig. 10 Mossbauer spectra for ITP-10 sample

Also, the presence of a magnetic Fe^{2+} species (~27%) in te ITP11 sample was detected, having absorption lines at +/- 4.5 mm/s. In the same sample, Mossbauer analysis show also a paramagnetic component as a central line with near zero velocitym, attributed to Fe^{3+} species. Room temperature (295 K) Mossbauer analysis of ITP10 shows a dpublet with a small splitting QS=0.80 mm/s – attributed to Fe3+ and another doublet with QA=2.48 mm/s, attributed to Fe^{2+} (~44%) .

As conclusions:

- The analyzed samples show the presencxe of bivalent iron species
- At high iron and (low silicon) concentrations –ITP10 sample there are no significant magnetic species from Mossbauer analysis at room temperature
- At higher Si atomic concentration (ITP11 sample) , at low temperature (5K) there are indications of Fe^{2+} species presence
- Trivalent iron (Fe^{3+}) species are spinelic tupe

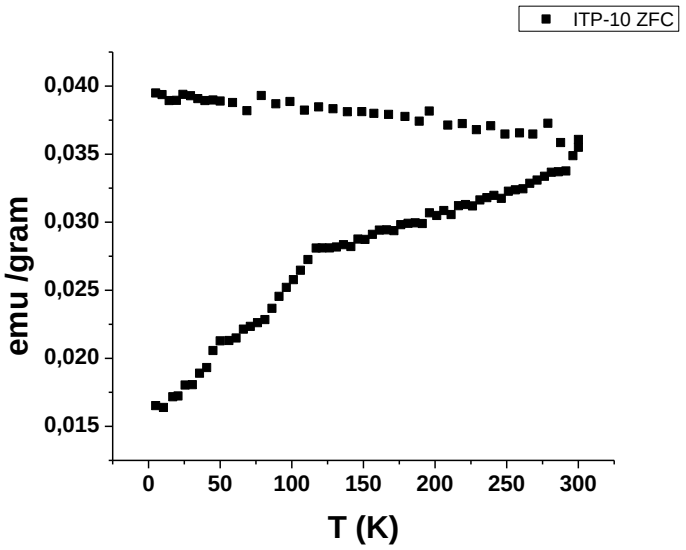

Fig .11. ZFC-FC for ITP10 sample

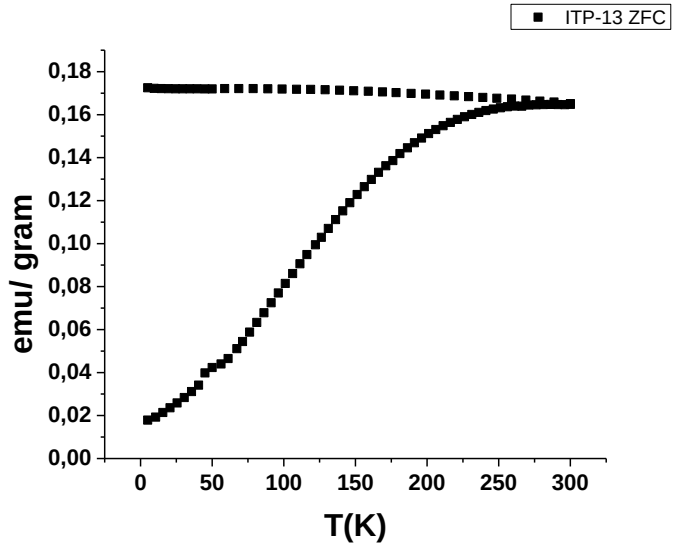

Fig. 12. ZFC-FC for ITP-13 sample

Measuring the magnetism during temperature variance without external fields (zero field cooling ZFC) and in the presence of external magnetic field (field cooling FC) - fig. 12 - allow us to draw some conclusions

a. For the ITP13 sample, richer in silicon, presenting a significant magnetization , there are iron species most probable associated with silicon

b. There are a visible maximum (sample ITP10) in ZFC (Fig.11) which indicate a clusterization of iron-containing entities, correlated with higher iron content (three times more) towards ITP13 sample

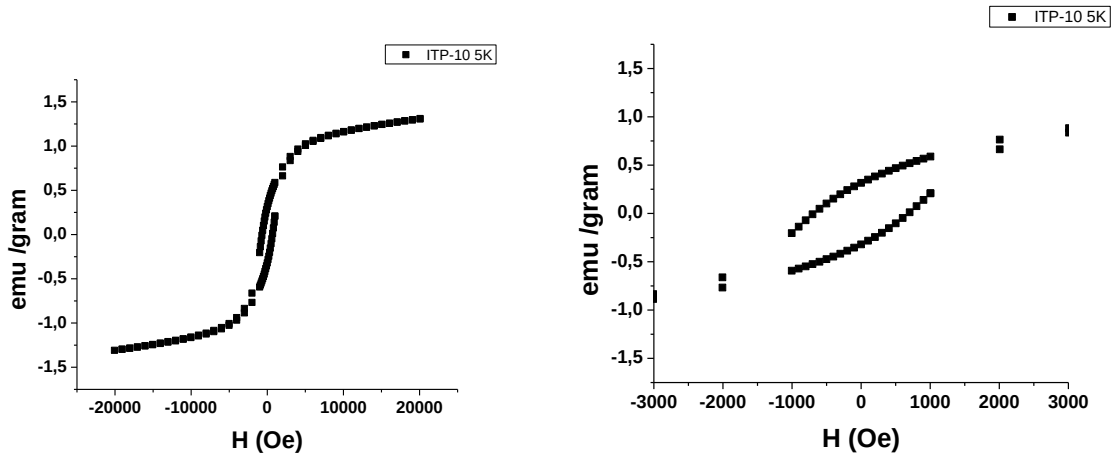

Fig.13. Magnetization curves at 5 K for ITP-10 sample

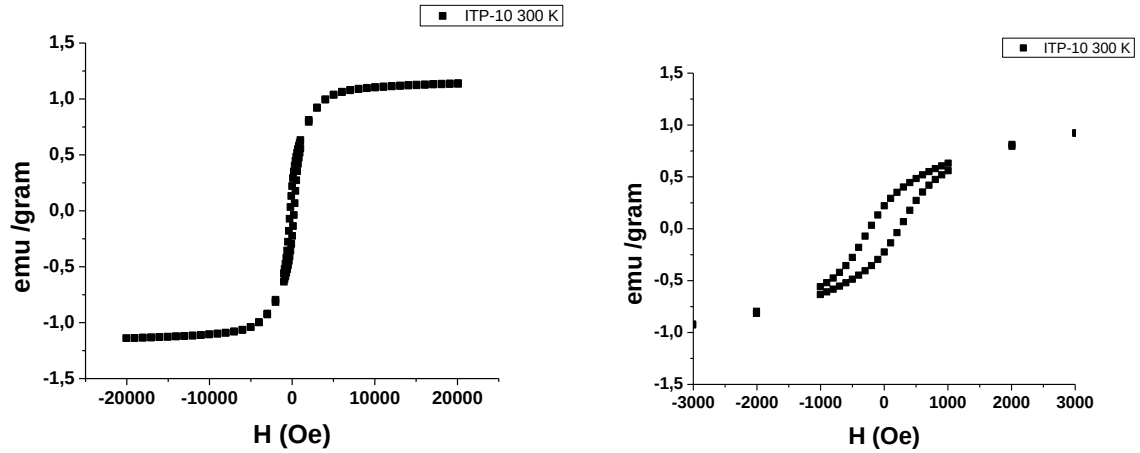

Fig.14. Magnetization curves at 300 K, ITP-10 sample

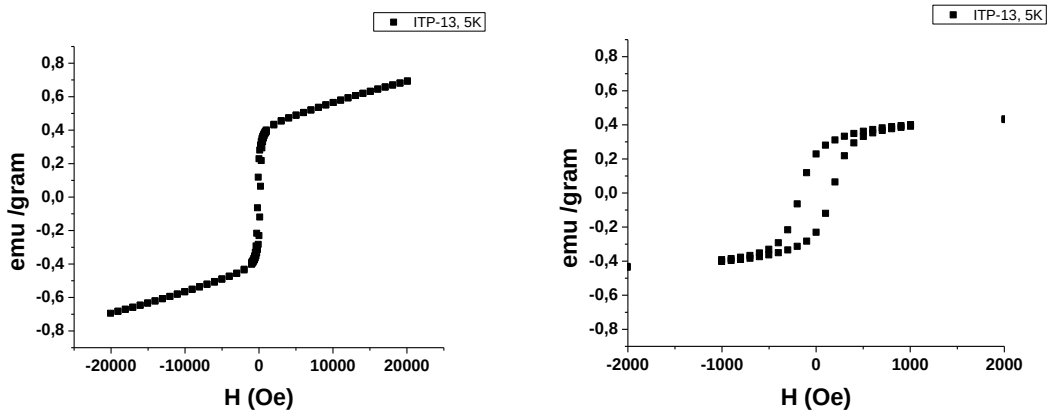

Fig.15 Magnetization curves at 5 K, ITP-13 sample

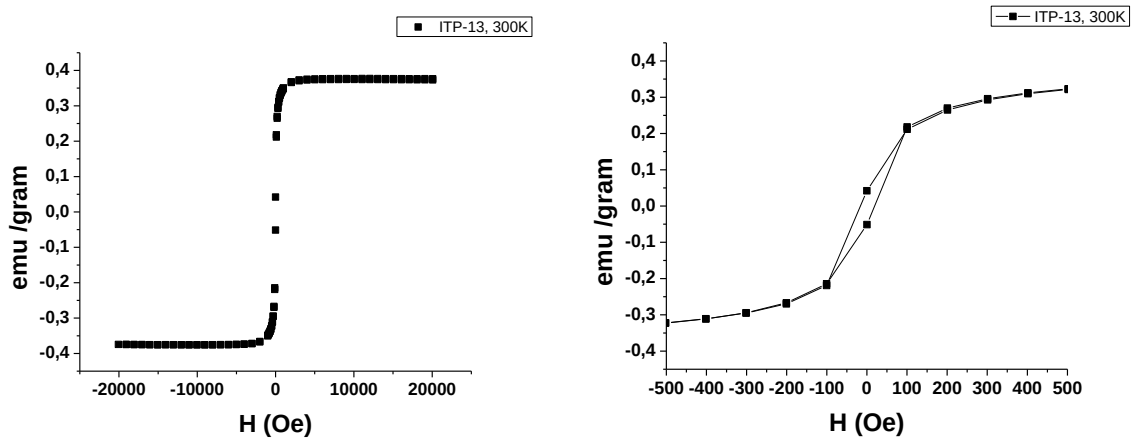

Fig.16 Magnetization curves at 300 K, ITP-10 sample

Magnetization curves corresponding to ITP10 and ITP13 samples at low temperature and at room temperature presented above (fig. 13-16) allow us to extract some important aspects:

a. There are antiferromagnetic couplings, resulting in principal for 5 K curves
b. The coercitive fields (forces) are enhanced with lowering the temperature
c. The magnetization is dependent to the amount of iron in the sample (see EDX), depending also to the nature of the magnetic species, presuming also the formation of chemical entities containing both Fe ands Si
d. The clusterization tendency , with the foremation of multicentric systems having very close magnetic centers induced by the relative high amount of Fehave an important role
e. A very small coercivity - indicating a near superparamagnetic phase appears at room temperature for ITP13 sample

Comparison of the results withdata from literature regarding the magnetic properties from TiO_2 systems having iron-based phases (such as magnetic oxides)

The literature concerning titania-based photocatalysts having also magnetic properties cite many systems that contain nano-iron oxides or nanoferites which gives them the opportunity to be manipulates with the aid of external magnetic fields, allowing thus a facile recover of the suspended photocatalysts and their possible recycling, In the following table 9, the performances and composition of such systems were resumed.

Table 9. Examples of magnetic titania-based photocatalysts from literature

Magnetic/photocatalytic system	**Reference**	**Saturation magnetization [emu/g]**	**Coercivity [Oe]**	**Observed (non)crystalline phases**	**Reciclability/ photodegraded substance/ Employed radiation**
TiO_2 mesoporuos submicronic particles + coloidosome-assembled iron oxide nanoparticles (colloidal crystals)	[M01]	2.8	~ 0(super-paramag.)	anatase, αFe_2O_3	5 cycles/ Orange II dye, /UV radiation
Titania-silica nanocomposite having various molar content of cobalt ferrite (SiO_2:Co = 0.004;0.008;0.016;0.032	[M02]	38.3; 22.9; 43.5; 15.8	299; 332; 484; 299	TiO_2-SiO_2 amorphous, $CoFe_2O_4$	6 cycles / Methylene blue dye /radiation
Titania – cobalt ferrite nanocomposite	[M03]	0.18	~1100	rutil, $CoFe_2O_4$, Co_3O_4, αFe_2O_3	1cycle/Reactive Red 120 dye/ visible radiation (W filament)
Core-shell nanocomposite having the iron oxide nanoparticles core covered with silica and then with titania	[M04]	46.5	<200 G	anatas, Fe_3O_4, SiO_2 amorf	1 cycle/ Methyl-orange dye/UV and Visi-ble radiation
Cobalt ferrite nanofibers covered with nanotitania	[M05]	33.2	894 G	anatas, rutil, $CoFe_2O_4$, $CoTiO_3$, $FeTiO_3$	1 cycle/Methylene blue dye / UV radiation
Core-shell nanocomposite having the iron oxide nanoparticles core covered with silica and then with mesoporous titania	[M06]	38.7	~ 0 (super-paramag.)	anatas, Fe_3O_4,	10 cycles / Rhodamine B dye/UV radiation
Core-shell nanocomposite having the iron oxide nanoparticles core covered with silica and then with titania	[M07]	28	~ 0 (super-paramag.)	anatase, rutile, Fe_3O_4,	1 cycle/ benzoic acid/ UV radiation
Iron oxide submicron spheres	[M08]	56.1	~ 0 (su-	anatase,	5 cycles /

wrapped in carbon and covered with titania nano-particles as nanocomposite			per-para-mag.)	Fe_3O_4,	Methylene blue dye/UV radiation
Porous silica impregnated with iron oxide nanoparticles (10 sau 15 Fe wt. %) and covered with titania	[M09]	3.72; 5.33	~ 0 (su-per-para-mag.)	anatase, rutile, Fe_3O_4,	1cycle/Reactive Briliant Red X-3B/ UV and Visible radiation
Spherical submicron aggregates of compacted nano-iron oxide covered with a common titania shell	[M10]	high	~ 0 (su-per-para-mag.)	anatase, Fe_3O_4	18 cycles/ Rhodamin B dye / UV radiation
Active carbon particles impregnated with titania and ZnMn ferrite nanoparticles	[M11]	10.1	5.22	anatase, rutile, $MnZnFe_2O_4$	5 cycles/ Methylorange/ UV radiation
Nanocomposite from aggregated titania si magnetite noparticles having a TiO_2:Fe_3O_4 molar ratio of 4; 8 sau 10	[M12]	46.4; 28.9; 13.7	0.0003 0.0004 0.0011 super-parmag	anatase, Fe_3O_4	1 cycle / Methylene Blue dye / UV radiation
Nanocomposite from titania si magnetite combined nano-particles (using opposite charged electrolytes) (3, 8, 13, 20, 30 wt.% maghemite)	[M13]	11.4	~20 (~ su-per-para-mag.)	anatase, rutile, Fe_3O_4,	4 cycles / insecticide propachlor/ UV radiation
Nanocomposite from nano cobalt ferrite covered with a nitrogen-doped titania shell	[M14]	~2.8; ~3.7; ~5.6; ~6.1	~1380; ~1380; ~2350 ~2350	anatase, $CoFe_2O_4$,	3 cycles / Methylene Blue dye / UV radiation
Active carbon impregnated with spinellic iron oxide nanoparticles covered with nitrogen-doped titania	[M15]	~7	~ 0(su-per-para-mag.)	anatase, γFe_2O_3	6cycles/Briliant Reactive Red X-3B dye/ UV and Visible, radiation (Solar)
Active carbon particles impregnated with spinellic iron oxide nanoparticles covered with titania (maghemite : carbon weight ratios 1:5 or 1:7	[M16]	2.2; 1.2	12; 11	anatase, γFe_2O_3	6 cycles /phenol / UV radiation
	[M17]	6.5	12.5		1 cycle/phenol / UV radiation
Nickel ferriyte nanoparticles covevered with silica and combined with nanotitania	[M18]	~1	~10(~ su-per-para-mag.)	anatase, rutile, $NiFe_2O_4$,	3 cycles / Metilorange dye/ UV radiation

As can be observed, the magnetic properties of the titani-based systems containing iron oxidic phases are very different, having maximum saturation magnetization at room temperature values

not far from 50 emu/g due to the dilution of the intrinsic magnetism of the magnetic particles wioth non-magnetic materials provided by titania (and sometimes by silica and carbon). Also. There are many report of low magnetization saturation values (under 6 emu/g) similar with those reported for our titania-based samples having magnetic phases synthesized by laser pyrolysis. Rven if they appear to be small, these valus are sufficient for the magnetic-field induced separattion (and recycling) of these particles from aqueous suspensions. Regarding the values of coercivity, one can observe that the great majority of the magnetic photocatalytic nanocomposites are superparamagnetic or have a behaviour very near too superparamagnetism, a positive feature translated in the lack of magnetic attraction between particles in the absence of an external magnetic field, which could induce apremature agglomeration in suspensions and to a reduiction of light absobption required by the photocatalytic processes.

Bibliography

[M01] J.E. Chen, H.-Y. Lian,S. Dutta, S.M. Alshehri,Y. Yamauchi, M.T. Nguyen, T. Yonezawa, K.C.-W. Wu, Synthesis of magnetic mesoporous titania colloidal crystals through evaporation induced
self-assembly in emulsion as effective and recyclable photocatalysts, Phys.Chem.Chem.Phys. 17(2015) 27653-26657.

[M02] F.A. Harraz, R.M. Mohamed, M.M. Rashad, Y.C. Wang, W. Sigmund, Magnetic nanocomposite based on titania–silica/cobalt ferrite for photocatalytic degradation of methylene blue dye, Ceramics International 40 (2014) 375–384.

[M03] P. Sathishkumar, R. V. Mangalaraja, S. Anandan, M. Ashokkumar, $CoFe_2O_4/TiO_2$ nanocatalysts for the photocatalytic degradation of Reactive Red 120 in aqueous solutions in the presence and absence of electron acceptors, Chem. Eng. J.220 (2013) 302–310.

[M04] C. Xue, Q. Zhang, J. Li, X. Chou, W. Zhang, H. Ye, Z. Cui, P.J. Dobson, High photocatalytic activity of Fe_3O_4-SiO_2-TiO_2 functional particles with core-shell structure, J. Nanomaterials Vol. 2013, Article ID 762423, 8 pag..

[M05] C.-J. Li, J.-N. Wang, B. Wang, J.R. Gong , Z. Lin, A novel magnetically separable $TiO_2/CoFe_2O_4$ nanofiber with high photocatalyticactivity under UV–vis light, Mater. Res. Bull. 47 (2012) 333–337.

[M06] Q. Yuan, N. Li, W. Geng, Y. Chi, X. Li, Preparation of magnetically recoverable $Fe_3O_4@SiO_2@meso\text{-}TiO_2$ nanocomposites with enhanced photocatalytic ability, Mater. Res. Bull. 47 (2012) 2396-2402.

[M07] T.-L. Su, C.-S. Chiou, H.-W. Chen, Preparation, photocatalytic activity, and recovery of magnetic photocatalyst for decomposition of benzoic acid, Int. J. Photoenergy Vol.2012, Article ID 909678, 8 pag..

[M08] F. Shi, Y. Li, Q. Zhang, H. Wang, Synthesis of $Fe_3O_4/C/TiO_2$ Magnetic photocatalyst via Vapor Phase Hydrolysis, Int. J. Photoenergy Vol.2012, Article ID 365401, 8 pag..

[M09] C. Wang, Y. Ao, P. Wang, J. Hou, J. Qian, A facile method for the preparation of titania-coated magnetic porous silica and its photocatalytic activity under UV or visible light, Colloids Surf. A 360 (2010) 184–189.

[M10] M. Ye, Q.Zhang, Y.Hu, J. Ge, Z. Lu, L. He, Z. Chen, Y. Yin, Magnetically recoverable core–shell nanocomposites with enhanced photocatalytic activity, Chem. Eur. J. 2010, 16, 6243 – 6250.

[M11] S. Wang, S. Zhou, Titania deposited on soft magnetic activated carbon as a magnetically separable photocatalyst with enhanced activity, Appl. Surf. Sci. 256 (2010) 6191–6198.
[M12] L. Yuxiang, Z.Mei, G. Min, W. Xidong, Preparation and properties of a nano TiO_2/Fe_3O_4 composite superparamagnetic photocatalyst, Rare Metals 28 (2009) 423-427.
[M13] V. Belessi, D. Lambropoulou, I. Konstantinou, R. Zboril, J. Tucek, D. Jancik, T. Albanis, D. Petridis, Structure and photocatalytic performance of magnetically separable titania photocatalysts for the degradation of propachlor, Appl. Catal. B 87 (2009) 181–189.
[M14] H. Li, Y. Zhang, S. Wang, Q. Wu, C. Liu, Study on nanomagnets supported TiO2 photocatalysts prepared by a sol–gel process in reverse microemulsion combining with solvent-thermal technique, J. Hazard. Mater.169 (2009) 1045–1053.
[M15] Y. Ao, J. Xu, S. Zhang, D. Fu, Synthesis of a magnetically separable composite photocatalyst with high photocatalytic activity under sunlight, J. Phys. Chem. Solids 70 (2009) 1042–1047.
[M16] Y. Ao, J. Xu, Degang Fu, X. Shen, C. Yuan, A novel magnetically separable composite photo-catalyst: Titania-coated magnetic activated carbon, Sep. Purif. Technol. 61 (2008) 436–441.
[M17] Y. Ao, J. Xu, X. Shen, D. Fu, C. Yuan, Magnetically separable composite photocatalyst with enhanced photocatalytic activity, J. Hazard. Mater. 160 (2008) 295–300.
[M18] X. Shihong, S. Wenfeng, Y. Jian, C. Mingxia, S. Jianwei, Preparation and photocatalytic properties of magnetically separable TiO_2 supported on Nickel ferrite, Chin. J. Chem. Eng. 15 (2007)190—195.

Managerial activity, dissemination - year 2015

Articles published inISI-quoted journals (submitted in 2014):

C.T. Fleaca, M. Scarisoreanu, I. Morjan, C. Luculescu, A.-M. Niculescu, A. Badoi, E. Vasile, G. Kovacs "**Laser oxidative pyrolysis synthesis and annealing of TiO_2 nanoparticles embedded in carbon-silica shells/matrix**" *Appl. Surf. Sci.* 336 (2015) 226-233

M. Scarisoreanu, C.-T. Fleaca, , I. Morjan., I.P. Morjan, A-M..Niculescu, E. Dutu, A.Badoi, R. Birjega, C. Luculescu, E. Vasile, V. Danciu, G. Filoti "**Synthesis and photocatalytic properties of novel multifunctional TiO_2-based magnetic nanocomposite** *Appl. Surf. Sci.* 336 (2015) 335-342

Conferences International dissemination:

1. M. Scarisoreanu, C. Fleaca, I. Morjan, A.-M. Niculescu, C. Luculescu, I.P. Morjan, E. Dutu, A. Badoi, A. Ilie, E. Vasile, V. Danciu "One-step synthesis of TiO_2/SnO_2 nanocomposites and their photocatalytic performance" E-MRS Spring Meeting, Lille, France, May 11-15, 2015

2. C. Fleaca, M. Scarisoreanu, I. Morjan, C. Luculescu, A.-M. Niculescu, A. Badoi, E. Vasile, V. Danciu "Characterization and photocatalytic properties of blue core-shell $TiO_2/SiO_2/C$ nanocomposites obtained via laser pyrolysis" 11thInt. Conf. "Micro- to Nano-Photonics IV-ROMOPTO 2015", Bucharest, Romania, September 1-4, 2015

Project Coordinator,

Dr. Claudiu Fleaca